A New Approach for Quantitative Phosphoproteomic Dissection of Signaling Pathways Applied to T Cell Receptor Activation*

Vinh Nguyen‡§, Lulu Cao¶§, Jonathan T. Lin‡§, Norris Hung‡, Anna Ritz‖**, Kebing Yu¶, Radu Jianu‖, Samuel P. Ulin‡, Benjamin J. Raphael‖**, David H. Laidlaw‖, Laurent Brossay‡‡, and Arthur R. Salomon‡¶§§¶¶

Reversible protein phosphorylation plays a pivotal role in the regulation of cellular signaling pathways. Current approaches in phosphoproteomics focus on analysis of the global phosphoproteome in a single cellular state or of receptor stimulation time course experiments, often with a restricted number of time points. Although these studies have provided some insights into newly discovered phosphorylation sites that may be involved in pathways, they alone do not provide enough information to make precise predictions of the placement of individual phosphorylation events within a signaling pathway. Protein disruption and site-directed mutagenesis are essential to clearly define the precise biological roles of the hundreds of newly discovered phosphorylation sites uncovered in modern proteomics experiments. We have combined genetic analysis with quantitative proteomic methods and recently developed visual analysis tools to dissect the tyrosine phosphoproteome of isogenic Zap-70 tyrosine kinase null and reconstituted Jurkat T cells. In our approach, label-free quantitation using normalization to copurified phosphopeptide standards is applied to assemble high density temporal data within a single cell type, either Zap-70 null or reconstituted cells, providing a list of candidate phosphorylation sites that change in abundance after T cell stimulation. Stable isotopic labeling of amino acids in cell culture (SILAC) ratios are then used to compare Zap-70 null and reconstituted cells across a time course of receptor stimulation, providing direct information about the placement of newly observed phosphorylation sites relative to Zap-70. These methods are adaptable to any cell culture signaling system in which isogenic wild type and mutant cells have been or can be derived using any available phosphopeptide enrichment strategy. ***Molecular & Cellular Proteomics 8:2418–2431, 2009.***

From the ‡Department of Molecular Biology, Cell Biology, and Biochemistry, ¶Department of Chemistry, ‖Department of Computer Sciences, **Center for Computational Molecular Biology, ‡‡Department of Molecular Microbiology and Immunology, and §§Center for Genomics and Proteomics, Brown University, Providence, Rhode Island 02912

Received, July 7, 2008, and in revised form, July 7, 2009

Published, MCP Papers in Press, July 14, 2009, DOI 10.1074/mcp.M800307-MCP200

The reversible phosphorylation of serine, threonine, and tyrosine residues directly controls many cellular processes, leading to the activation of a coordinated network of additional phosphorylation events across multiple proteins over time. Clearly, there are benefits to individually identifying and characterizing specific components of a particular pathway, such as a phosphorylation site on a given protein, the kinase responsible for the modification, or the proteins interacting subsequently. However, a thorough understanding of these signaling pathways at the molecular level ultimately requires a global, simultaneous evaluation of these phosphorylation events as they occur over time.

Currently, the most common method for assessing wide-scale changes in the proteome is two-dimensional gel electrophoresis (1), but this methodology is relatively low throughput and not optimal for the analysis of low abundance and hydrophobic signaling proteins (2). Recent publications describe alternate approaches for assessing changes in phosphorylation patterns based primarily on LC/MS methodologies (3–8). A variety of promising purification approaches have been developed to discover hundreds to thousands of phosphorylation sites from complex cell lysates including strong cation exchange/titanium dioxide (SCX/TiO_2), IMAC[1], and IMAC in tandem with phosphotyrosine peptide immunoprecipitation (3, 4, 6, 9–12). These phosphoproteomic methods have been used to survey a large number of phosphorylation sites in a time course after receptor stimulation, where the magnitude of-fold change in phosphorylation and the

[1] The abbreviations used are: IMAC, immobilize metal affinity chromatography; ADAP, adhesion and degranulation adaptor protein; CD, cluster of differentiation; Erk1/2, extracellular signal-regulated kinase-1/2; ITAM, immunoreceptor tyrosine activation motif; ITK, interleukin-2-inducible T cell kinase; LAT, linker for activation of T cells; Lck, lymphocyte-specific protein tyrosine kinase; NTBA, natural killer-, T- and B-cell antigen; MAPK, mitogen-activated protein kinase; PBS, phosphate buffered saline; PH, pleckstrin homology; PLCγ1, phospholipase C gamma 1; SHP-1/2, SH2 domain-containing protein tyrosine phosphatase-1/2; SIC, selected ion chromatogram; SILAC, stable isotopic labeling of amino acids in cell culture; SKAP55, src kinase-associated phosphoprotein of 55 kDa; TCR, T cell receptor; Zap-70, zeta-chain-associated protein kinase 70; ITIM, immunoreceptor, the tyrosine-based inhibitory motif; FTMS, Fourier transform mass spectrometer.

timing of phosphorylation suggest protein participation and placement within a pathway (6, 10, 12–14). For example, proteins phosphorylated late after receptor stimulation are expected to represent downstream elements of a pathway whereas rapid phosphorylation is expected in the earlier stages of a pathway, especially at the receptor. Constitutive phosphorylation throughout a receptor stimulation time course is expected for proteins not involved in the pathway (10).

Although receptor stimulation time course experiments provide clues about placement of phosphorylation sites within a pathway relative to a stimulated receptor, a phosphoproteomic analysis comparing signaling protein null mutants and their reconstituted counterparts would allow for precise placement of novel phosphorylation sites within a signaling pathway relative to signaling landmarks within the canonical pathway (Fig. 1). An ideal quantitative method to perform this analysis would provide both a dense temporal array of information about protein phosphorylation after receptor stimulation as well as precise comparisons between isogenic matched normal cells and cells with altered signaling proteins.

Quantitation in proteomics experiments facilitates the comparison of proteins between various cellular states such as a receptor stimulation time course experiment. Stable Isotope Labeling of Amino Acids in Cell Culture (SILAC) is an effective method for measuring the relative abundance of proteins in cell or tissue samples (15). In the SILAC technique, heavy or light essential amino acids are incorporated into cellular proteins through metabolic labeling in cell culture before cellular stimulation. This method allows for normalization of errors through the entire process of stimulation of cells, purification of proteins, and acquisition of LC/MS data, providing precise measurements of small differences between samples (15). However, the number of comparisons possible in a single experiment is often limited in practice by the number of labeled amino acids available (16). The number of cellular state comparisons may be extended beyond the limits of available labeled amino acids by label-free quantitation using repetition of biological stimulations in separate SILAC experiments (6) or normalization to spiked phosphopeptide standards. Label-free quantitation between separate LC/MS experiments is facilitated by automation of peptide chromatography and data acquisition, resulting in enhanced reproducibility of chromatographic retention times and peak areas (17). The automated IMAC/nano-LC/ESI-MS system used here provides the necessary reproducible peak areas (8% relative standard deviation) and retention times (0.2% relative standard deviation) (17). The combination of SILAC and label-free quantitation allows for a greatly increased number of receptor stimulation time points while providing highly accurate comparisons between signaling protein null and reconstituted cells at each time point using SILAC.

Because of its high degree of prior characterization, the T cell receptor (TCR) signaling pathway is an ideal model system for validating our approach for quantitative phosphoproteomic analysis of isogenic signaling pathway mutants. TCR signaling plays an essential role in regulating the adaptive immune response, and many proteins involved in the pathway have been identified (Fig. 1) (18–20). The availability of the highly characterized Jurkat leukemic T cell line has greatly facilitated investigations of TCR signaling by traditional and phosphoproteomic methods (13, 21). Furthermore, many isogenic disruption mutants of essential TCR signaling proteins have been isolated through genetic screens of mutagenized Jurkat clones, revealing severe phenotypic defects in TCR signaling and function (22–26). In particular, P116, a Zap-70 null clone, displays defects in stimulus-induced calcium mobilization, interleukin-2 production, nuclear factor of activated T cells transcription activation, and protein tyrosine phosphorylation on PLCγ1, ITK, LAT, Erk1/2, and SLP76 (25, 27–29). In the present study, a hybrid SILAC/label-free approach was applied to the P116 (Zap-70 null) and P116.c139 (Zap-70 reconstituted to wild type levels) Jurkat clones, and the placement of newly discovered tyrosine phosphorylation sites relative to Zap-70 was determined.

EXPERIMENTAL PROCEDURES

Cell Culture, SILAC Labeling, and T Cell Stimulation—Jurkat clones P116 (Zap-70 null) and P116.c139 (Zap-70 reconstituted) were provided by L. Samelson at the National Institute of Health. All cells were initially maintained in RPMI 1640 medium (Sigma) supplemented with 10% heat inactivated undialyzed fetal bovine serum (Hyclone, Logan, UT), 2 mM L-glutamine, 100 units/ml penicillin G, and 100 μg/ml streptomycin (Invitrogen) in a humidified incubator with 5% CO_2 at 37 °C. After 5 days, all cell lines were washed twice with RPMI 1640 medium without Arg and Lys (Invitrogen) and reconstituted in RPMI 1640 medium containing either $^{12}C_6$, $^{14}N_4$ Arg and $^{12}C_6$, $^{14}N_2$ Lys (Sigma) or $^{13}C_6$, $^{15}N_4$ Arg and $^{13}C_6$, $^{15}N_2$ Lys (Cambridge Isotope Laboratories, Andover, MA) supplemented with 10% heat-inactivated dialyzed fetal bovine serum (Sigma), 2 mM L-glutamine, 100 units/ml penicillin G, 100 μg/ml streptomycin in a humidified incubator with 5% CO_2 at 37 °C for 7 cell doublings. The concentration of Lys and Arg used in SILAC labeling of Jurkat cells in experiments described here was 0.22 mM and 0.38 mM, respectively.

Anti-CD3 and anti-CD4 (clones OKT3 and OKT4; eBioscience, San Diego, CA) stimulation was performed as described (13). Briefly, cells were washed once with 4 °C phosphate buffer saline (PBS), and reconstituted at a concentration of 1×10^8 cells/ml in PBS. For each time point, 1×10^8 cells were treated with OKT3 and OKT4 primary antibodies at a concentration of 2.5 μg/ml of each antibody for 10 min at 4 °C. Cells were then cross-linked with 22 μg/ml of goat anti-mouse IgG (Jackson ImmunoResearch, West Grove, PA) and incubated at 37 °C for 0, 2, 3, 5, 7, or 10 min.

Cell Lysis, Protein Reduction, Alkylation, Digestion, and Peptide Immunoprecipitation—To halt the stimulation, cells were placed in lysis buffer (8 M urea, 1 mM sodium orthovanadate, and 100 mM ammonium bicarbonate, pH 8.0) and incubated for 20 min at 4 °C. Lysates were then cleared at 12,000 $\times$ *g* for 15 min at 4 °C, and protein concentrations were measured by the DC Protein Assay (Bio-Rad). Once protein concentrations were determined, cell lysates from P116 and P116.c139 were combined at a 1:1 protein concentration ratio and reduced with 10 mM dithiothreitol for 1 h at 56 °C, followed by alkylation with 55 mM iodoacetamide for 1 h at room temperature. Cell lysates were then diluted 5-fold with 100 mM ammonium bicar-

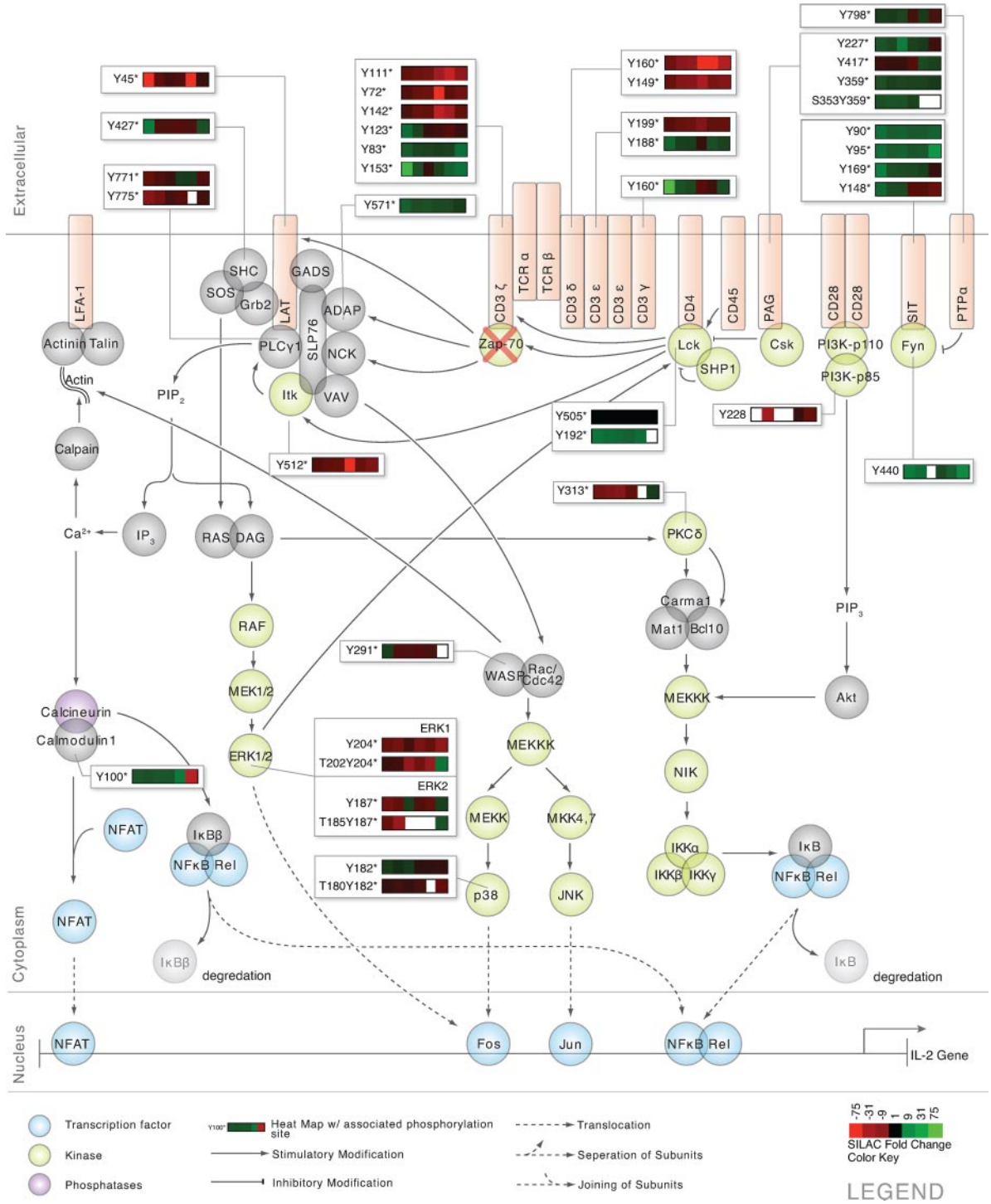

FIG. 1. **Canonical TCR signaling pathway.** Established signaling cascades in activated T cells with quantitative Zap-70 null/Zap-70 reconstituted SILAC ratio data represented as heatmaps besides individual proteins. Heatmaps represent averages of five replicate experiments. In the heatmap representation, *green* represents elevated phosphorylation in response to Zap-70 removal, whereas *red* represents a decrease in phosphorylation in response to Zap-70 removal. *Black* represents no change. *Blanks* in the heatmap indicate that a clearly defined SIC peak was not observed for that phosphopeptide in that time point. The utility of this visual representation is validated by the large number of *red* heatmap *bars* downstream of Zap-70 in the canonical pathway. Note that the * next to the phosphorylation site signifies that this site has been previously described in the literature.

bonate (pH 8.9) and digested with sequencing grade modified trypsin (Promega, Madison, WI) at a 1:100 (w/w) trypsin:protein ratio overnight at room temperature. Tryptic peptides were acidified to pH 2 with concentrated HCl, cleared at 2000 × *g* for 10 min at 22 °C, desalted using C18 Sep-Pak plus cartridges (Waters, Milford, MA) as described (14), and lyophilized in a SpeedVac plus (Thermo Fisher Scientific, Waltham, MA). A 100-pmol fraction of synthetic phosphopeptide LIEDAEpYTAK was added to each time point sample prior to peptide immunoprecipitation. Dry peptides from each time point were reconstituted and immunoprecipitated as described previously (10) except 20 μl of anti-phosphotyrosine resin was used per 1×10^8 cells and eluted peptides were filtered through a 0.22 μM filter (Millipore, Billerica, MA).

Results presented throughout this manuscript are collected from the average of five total replicate analyses for each time point. Two biological replicates from separate frozen stocks of P116 (Zap-70 null) and P116.c139 (Zap-70 reconstituted) cells were cultured in RPMI containing isotopic heavy or light amino acids. These biological replicates were performed ten months apart. The first biological replicate contained two technical replicates while the second biological replicate contained three technical replicates. Cells were stimulated, lysed, and SILAC labeled heavy (Zap-70 null) and light (Zap-70 reconstituted). Lysates were combined and digested with trypsin. For technical replicates, digested peptides from each time point were then divided into two or three equal fractions before desalting by C18 Sep-Pak plus cartridges and were kept separated throughout the rest of the experiment.

Western Blotting for Zap-70 and Phospho-Erk1/2—Total cellular protein from 8 M urea cell lysates was diluted 1:1 with gel loading buffer containing 4% SDS, 125 mM Tris-HCl (pH 6.8), 20% v/v glycerol, 5% 2-mercaptoethanol, 0.01% bromphenol blue, pH 6.8 from each proteomic sample. Equal amounts of protein (as measured by Lowry DC assay; Bio-Rad) were separated by 4–20% gradient SDS-polyacrylamide gel electrophoresis (Item 25204; Thermo Fisher Scientific), and electroblotted to an Imobilin membrane (Millipore). The membrane was blocked for 45 min in blocking buffer at 22 °C (PBS/Tween-20/5% milk) and then incubated for 12 h at 4 °C with 1:1000 of either rabbit anti-human phospho-p44/p42 MAPK (Thr-202/Tyr-204) or mouse anti-human Zap-70 antibody (Cell Signaling Technology, Danvers, Ma). The membrane was washed 4 × 10 min at 22 °C in PBS/Tweeen-20. The membrane was then stained with 1:3000 of anti-rabbit IgG or anti-mouse IgG directly conjugated to horseradish peroxidase (Cell Signaling Technology) for 1 h in blocking buffer at 22 °C and washed 5 × 15 min with PBS/Tween-20. Bands were visualized using chemiluminescence with the ECL kit (Amersham Biosciences).

Automated Desalt-IMAC/nano-LC/ESI-MS—Tryptic peptides were analyzed by a fully automated phosphoproteomic technology platform integrating peptide desalting via reversed-phase chromatography, and Fe^{3+} IMAC enrichment of phosphopeptides as previously described (10). IMAC-enriched phosphopeptides were eluted into the mass spectrometer (Linear Trap Quadrupole-Fourier Transform (LTQ-FT)) (Thermo Fisher Scientific) through an analytical column (360 μm outer diameter × 75 μm inner diameter-fused silica with 12 cm of 5 μm Monitor C18 particles with an integrated ~4 μm-ESI emitter tip fritted with 3-μm silica; Bangs Laboratories) with a reversed-phase gradient (0–70% solvent B in 30 min). Static peak parking was performed via flow rate reduction from 200 nl/min to ~20 nl/min when peptides began to elute as judged from a bovine serum albumin peptide scouting run, as described previously (17). Using a split flow configuration, an electrospray voltage of 2.0 kV was applied as described (30). Spectra were collected in positive ion mode and in cycles of one full MS scan in the Fourier Transform (*m/z* 400–1800) followed by data-dependent MS/MS scans in the LTQ (~0.3 s each), sequentially of the five most abundant ions in each MS scan with charge state screening for +1, +2, +3 ions and dynamic exclusion time of 30 s. The automatic gain control was 1,000,000 for the FTMS scan and 10,000 for the ion trap mass spectrometry scans. The maximum ion time was 100 ms for the ion trap mass spectrometry scan and 500 ms for the FTMS full scan. FTMS resolution was set at 100,000.

Database Analysis—MS/MS spectra were searched against the human National Center for Biotechnology Information non-redundant protein database using the SEQUEST algorithm provided with Bioworks 3.2 (SEQUEST v.27 rev12) (31). Peak lists were generated using Bioworks 3.2 (extract_msn.exe 11/27/06) using a mass range of 600–4500, precursor ion tolerance (for grouping) of 0.005 atomic mass unit, minimum ion count of 5, group scan of 0, minimum group count of 1. The NCBI human database contained 489,388 protein entries (50% forward, 50% reversed). SEQUEST was performed with the following parameters: trypsin enzyme specificity, 2 possible missed cleavages, 0.2 Da mass tolerance for precursor ions, 0.5 Da mass tolerance for fragment ions. Search parameters specified a differential modification of phosphorylation (+79.9663 Da) on serine, threonine, and tyrosine residues and a static modification of carbamidomethylation (+57.0215 Da) on cysteine. Search parameters also included a differential modification for arginine (+10.00827 Da) and lysine (+8.01420 Da) amino acids. To provide high confidence phosphopeptide sequence assignments, SEQUEST results were filtered by Xcorr (+1 > 1.5; +2 > 2.0; +3 > 2.5), precursor mass error (<20 ppm), and a logistic spectral score (32) that assessed MS/MS spectral quality (>0.7981), minimum peak area threshold of 500 SILAC and label-free quantitation were required, non-redundant phosphopeptides, and proteins with descriptors of "unnamed" or "unknown" were removed. Additionally, repeat observations of MS/MS spectra of each tyrosine phosphorylated peptide in minimally three of six total time points were required. False discovery rate was estimated with the decoy database approach after final assembly of nonredundant data into heatmaps (33). To validate the position of the phosphorylation site, the Ascore algorithm (34) was applied to all data, and the reported phosphorylation site position reflected the top Ascore prediction. Ascore probabilities are reported in the full data Table in supplemental material 6.

Quantitation of Relative Phosphopeptide Abundance—Relative quantitation of peptide abundance was performed via calculation of selected ion chromatogram (SIC) peak areas of heavy and light SILAC-labeled peptides. For label-free comparison of phosphopeptide abundance in the Zap-70 reconstituted Jurkat cells, individual time point SICs were normalized to the LIEDAEpYTAK peak area in the same time point. The standard exogenous LIEDAEpYTAK peptide accompanied cellular phosphopeptides through the peptide immunoprecipitation, desalt, IMAC, and reversed-phase elution into the mass spectrometer. Peak areas were calculated by inspection of SICs using recently developed software programmed in Microsoft Visual Basic 6.0 based on Xcalibur Development kit 2.0 SR2 (Thermo Fisher Scientific). Quantitative data was calculated automatically for every assigned peptide using the ICIS algorithm available in the Xcalibur XDK with the following parameters: multiple resolutions of 8, noise tolerance of 0.1, noise window of 40, scans in baseline of 5, Include of RefExc Peaks is False. A minimum SIC peak area equivalent to the typical spectral noise level of 500 was required of all data reported for label-free and SILAC quantitation.

A label-free data heatmap was generated for comparison of phosphopeptides in Zap-70 reconstituted Jurkat cells through a time course of receptor stimulation. The magnitude of change of the heatmap color was calculated from the log of the ratio of the-fold change of each individual peptide peak area compared with the geometric mean for that peptide across all time points (as described in detail in

supplemental material 7). Any changes (either an increase or decrease of peptide abundance above the average) with greater than 75 maximal -fold change were displayed as the same color as the 75 maximal -fold change. In the heatmap representation, the geometric mean of a given phosphopeptide across all time points was set to the color black. A blue color represented below average abundance, while yellow represented above average abundance for each unique phosphopeptide. Blanks in the heatmap indicated that a clearly defined SIC peak was not observed for that phosphopeptide in any of the replicate analyses for that time point. The heatmap colors were generated from the average of the LIEDAEpYTAK standard peptide normalized SICs in the five replicate experiments. The coefficient of variation was calculated for each heatmap square (supplemental material 6). *p* values were also calculated between the replicate distributions of each heatmap square compared with the time point with the minimal average value for that phosphopeptide (supplemental material 6).

In the second type of heatmap, SILAC ratios corresponding to peptide abundance differences between Zap-70 null and reconstituted cell lines across the time course of receptor stimulation were represented. For the SILAC heatmaps, a black color represented a ratio of 1 between the two cell lines for a given peptide at that time point. A red color represented less abundance, and green represented higher abundance of the given peptide in the Zap-70 null cells compared with the Zap-70 reconstituted cells. The magnitude of change of the heatmap color was calculated as described in detail in supplemental material 8. The heatmap color was threshold at a maximal -fold change of 75-fold increased or decreased in the Zap-70 null cells compared with reconstituted cells. The coefficient of variation percent was calculated for each SILAC ratio heatmap square among the 5 replicate analyses (supplemental material 6). *p* values were also calculated between the Zap-70 null and Zap-70 reconstituted replicate measurements for each phosphopeptide and time point (supplemental Table 6).

RESULTS

Prior to analysis of Zap-70 null Jurkat cells, Jurkat cells were incubated with either 0.3 mM $^{13}C_6$, $^{15}N_4$ Arg or 0.18 mM $^{13}C_6$, $^{15}N_2$ Lys in dialyzed serum for 7 doublings to test the SILAC labeling conditions. Tyrosine phosphorylated peptides were enriched according to the standard peptide immunoprecipitation procedure described under "Experimental Procedures". After desalt, IMAC, and LC/MS, the phosphopeptides were identified with SEQUEST and filtered as described under "Experimental Procedures" to compile a nonredundant list of tyrosine phosphopeptides. In the $^{13}C_6$, $^{15}N_4$ Arg and $^{13}C_6$, $^{15}N_2$ Lys labeled samples a total of 130 and 111 nonredundant phosphopeptides were observed, respectively. There were no unlabeled peptides observed. In the $^{13}C_6$, $^{15}N_4$ Arg labeled sample, a single $^{13}C_5$, $^{15}N_1$ Pro was observed out of a total of 75 peptides that contained unlabeled proline (supplemental material 5).

To evaluate its utility, our quantitative phosphoproteomic approach was applied to the human Jurkat T cell clones, P116 (Zap-70 null) and P116.c139 (Zap-70 reconstituted to wild type levels). The removal of Zap-70 protein and decrease in phosphorylation in Erk1/2 in Zap-70 null and reconstituted cells by Western blot was consistent with previous reports on these Jurkat clones (supplemental material 1) (25, 27–29). A distribution of six time points was used to detect subtle fluctuations in the timing of phosphorylation. Zap-70 null to Zap-70 reconstituted SILAC phosphopeptide ratios were calculated at each time point in a time course of TCR stimulation (Fig. 2). Before peak area quantitation and SILAC ratio calculation, high-quality sequence assignments were first determined using stringent criteria (Xcorr $+1 > 1.5$; $+2 > 2.0$; $+3 > 2.5$; precursor mass error < 20 ppm, logistic spectral score > 0.7981 (32), minimum SIC peak area threshold of 500 for SILAC and label-free quantitation were required, tyrosine phosphorylated, with observations of each peptide MS/MS spectra in at least three of the six time points). The false discovery rate estimated from decoy database search was 2.22% after all filtering and assembly of non-redundant data into heatmaps. A total of five replicate experiments were performed (as described under "Experimental Procedures"). Quantitative comparisons were generated from SIC peak areas, and heatmaps were generated from the average values from all replicates. The complete list of quantitative replicate data, calculated coefficient of variation and *p* values are available (supplemental material 6).

Representation of Label-free and SILAC Quantitation—Two different visual representations in the form of heatmaps of quantitative data were generated for each sequenced phosphopeptide to reflect either the label-free or SILAC ratio data. These two heatmaps provide the relationship between each phosphopeptide sequenced and TCR stimulation (label-free heatmaps) or the removal of Zap-70 (SILAC ratio heatmaps).

In the label-free heatmap, the abundance of each phosphopeptide in Zap-70 reconstituted cells was compared across the T cell receptor stimulation time course (Fig. 3 and supplemental material 2). This type of quantitative analysis is useful for determining whether newly discovered phosphorylation sites change in abundance after receptor stimulation, providing a list of candidate phosphorylation sites that may participate in the T cell signaling pathway. These data are represented in the form of a heatmap where black corresponds to the average abundance for a given peptide across all time points, yellow corresponds to phosphorylation levels above the average, and blue corresponds to phosphorylation levels below the average. As expected, for many of the phosphorylation sites already known to be involved in TCR signaling, phosphorylation levels increase after receptor stimulation followed by a steady decrease (Fig. 3).

In the second SILAC heatmap, SILAC ratios between Zap-70 null and reconstituted cells are represented for each phosphopeptide and time point (supplemental material 3). These data are represented in the form of a SILAC ratio heatmap, where green corresponds to an increase in phosphorylation, red corresponds to a decrease in phosphorylation, and black corresponds to no difference when Zap-70 is removed from Jurkat T cells for a given phosphopeptide at each time point. The intensity of the color reflects the relative magnitude of the change in phosphorylation. If phosphoryla-

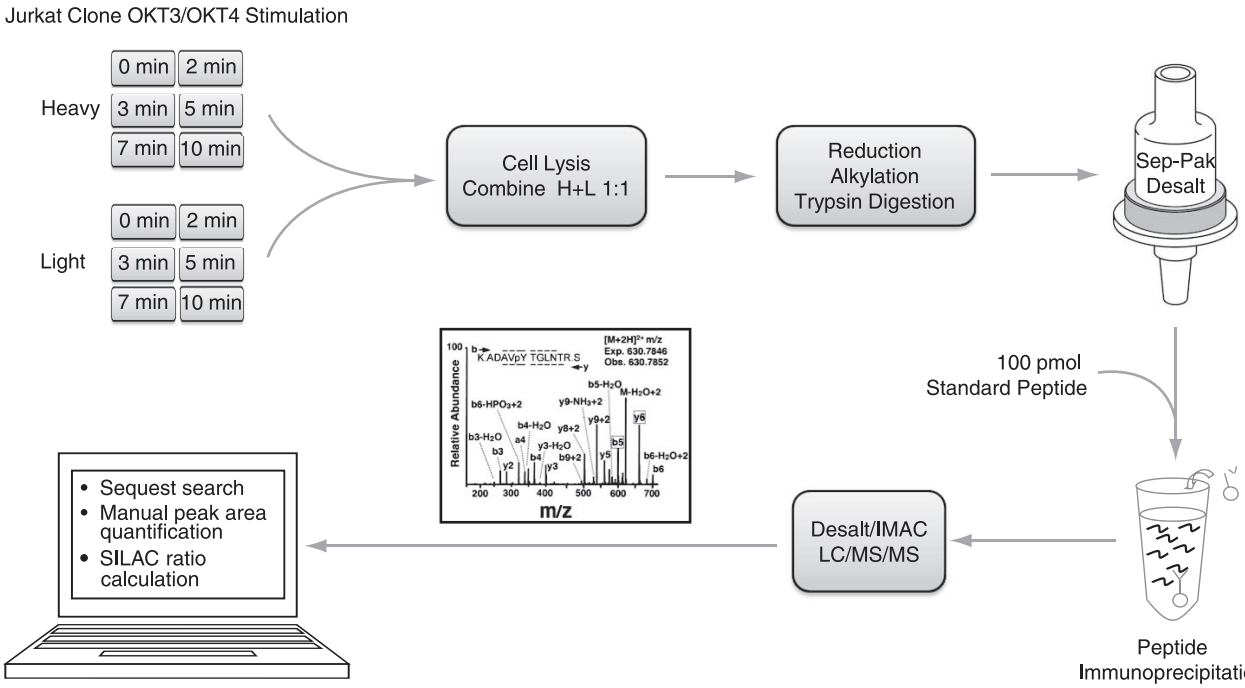

Jurkat clones	Weight	SILAC Labels and Mass Differences
P116.c139 (Zap-70 reconstituted)	Light	No labels on Arg or Lys
P116 (Zap-70 deficient)	Heavy	Arg ($^{13}C_6$, $^{15}N_4$) & Lys ($^{13}C_6$, $^{15}N_4$)

FIG. 2. **Experimental procedure.** Two cell populations of human Jurkat T cell clones (P116 and P116.c139) are incubated with normal or heavy isotope-labeled arginine and lysine amino acids, physically differentiating the two proteomes by a shift in molecular weights. Each cell population is then pre-incubated with OKT3 and OKT4 antibodies for 10 min at 4 °C and then cross-linked with IgG at 37 °C for the times indicated. After cell lysis, samples are combined at an equal protein concentration ratio of 1:1. Samples are then reduced, alkylated, and trypsin-digested into peptides. Peptides are desalted by Sep-Pak cartridges and then enriched by phosphotyrosine peptide immunoprecipitation and Fe^{3+} IMAC. Peptides are then subjected to reversed-phase LC-MS/MS analysis.

tion decreases in cells lacking Zap-70 compared with wild type, the phosphorylation event can be hypothetically positioned downstream of this protein. We then assessed the utility of our isogenic mutant approach by investigating the correlation between the known structure of the T cell signaling pathway and the changes in phosphopeptide abundance upon the removal of Zap-70. The utility of the method is validated by the large number of red heatmap bars downstream of Zap-70 in the canonical pathway (Fig. 1), indicating Zap-70-dependent phosphorylation.

Phosphoproteomic Profiling of Phosphorylation Sites Identified in Receptor-stimulated Zap-70 Reconstituted Jurkat Cells—From this analysis, we observed 168 tyrosine phosphorylation sites residing on 135 unique proteins in the Zap-70 reconstituted T cells across 6 time points of receptor stimulation (Fig. 3 and supplemental material 2). Among the 135 proteins identified, 24% of them (32 proteins) were previously functionally characterized in TCR signaling (20, 35, 36). Phosphorylation sites were observed on the earliest upstream TCR signaling components (TCR-CD3 subunits $\gamma\delta\varepsilon\zeta$, tyrosine kinases Lck, Fyn, Zap-70), crucial adaptor proteins (LAT, ITK, PLCγ1), and downstream target proteins (phosphoinositide 3-kinase (PI3K), Erk1, Erk2, CD5) (Figs. 1 and 3).

Because phosphorylation sites that do not change in response to TCR stimulation are unlikely to be involved in the TCR pathway, we focused our analysis on sites that showed a change (greater than 3-fold change) across the TCR stimulation time course in reconstituted Jurkat T cells as measured by label-free quantitation. These TCR responsive sites were further classified into a variety of groups with the use of SILAC ratio data to determine the dependence of each site upon the absence or presence of Zap-70 (Fig. 4).

Clustering of Phosphorylation Sites by Zap-70 Null/Reconstituted SILAC Ratios—Among the phosphopeptides that showed an increase in abundance with TCR stimulation in the reconstituted T cell time course, SILAC ratios of Zap-70 null to Zap-70 reconstituted cells were classified into four categories (Fig. 4): elevated phosphorylation (greater than 2-fold induction in two or more time points), no differences in phosphorylation (between 2-fold induction and 2-fold reduction in four or more time points), slightly decreased phosphorylation (between 2 to 10-fold reduction in two or more time

Protein Name	Phosphosites	mins 0 2 3 5 7 10	Protein Name	Phosphosites	mins 0 2 3 5 7 10	Protein Name	Phosphosites	mins 0 2 3 5 7 10
ADAP	Y571*		ERK1	T202*Y204*		PKC-δ	Y313*	
Calmodulin 1	Y100*		ERK2	Y187*		PLC-γ1	Y771*	
CBL	S669Y674*		ERK2	T185*Y187*		PLC-γ1	Y775*	
CBL	S667Y674*		Fyn	Y420*		PTPα	Y798*	
CD3γ	Y160*		Fyn	Y440		RhoGEF2	Y894	
CD3δ	Y160*		GSK3-β	Y216*		SHC	Y427*	
CD3δ	Y149*		GSK3-β	Y216*S219		SHP-2	Y62*	
CD3ε	Y199*		ITK	Y512*		SIT	Y90*	
CD3ε	Y188*		LAT	Y45		SIT	Y95*	
CD3ζ	Y111*		Lck	Y505*		SIT	Y169*	
CD3ζ	Y72*		Lck	Y192*		SIT	Y148*	
CD3ζ	Y142*		p38	Y182*		SKAP55	Y142	
CD3ζ	Y123*		p38	T180*Y182*		WASP	Y291*	
CD3ζ	Y83*		p56DOK	Y299*		ZAP70	Y493*	
CD3ζ	Y153*		p62DOK	Y409*		ZAP70	Y492*	
CD5	Y453*		PAG	Y227*		ZAP70	Y492*Y493*	
CD84	Y299		PAG	Y417*		ZAP70	Y292*	
CD84	Y279		PAG	Y359*		ZAP70	S491Y493*	
CDK5	Y15*		PAG	S353Y359*		ZAP70	Y248	
ERK1	Y204*		PI3K C2β	Y228				

FIG. 3. **Quantitative phosphoproteomic analysis of known TCR signaling proteins in wild type cells.** Listed above is a portion of the data collected, representing the known TCR signaling proteins that were observed in our study of human Jurkat P116.c139 (Zap-70 reconstituted) cells. Temporal quantitative changes in phosphorylation state are represented as heatmaps, which represent averages of five replicate experiments. In the heatmap representation, *yellow* represents levels of phosphorylation above the average, while *blue* represents levels of phosphorylation below the average. *Black* represents average abundance for a certain peptide across all time points. *Blanks* in the heatmap indicate that a clearly defined SIC peak was not observed for that phosphopeptide in that time point. Note that the * next to the phosphorylation site signifies that this site has been described previously in the literature.

points), and significantly decreased phosphorylation (greater than 10-fold reduction in two or more time points). From this grouping of phosphopeptide SILAC ratios, 43% showed enhanced phosphorylation, 19% showed no difference, 24% showed slight decrease, 12% showed significant decrease, and 2% represented outliers, which did not fully fall into any of the four major categories yet generally displayed minimal change.

Proteins with phosphorylation sites in the minimal change group included proteins known to function upstream of Zap-70 (CD3ε, CD3ζ, Lck) (20), proteins known to function in other signaling pathways in T cells (GSK3β, phosphoprotein associated with glycolipid-enriched membrane protein (PAG)) (37, 38), and ones not known to function in TCR signaling (Filamin B, CDC2, ELMO1).

In general, sites with decreased phosphorylation levels in P116 (Zap-70 null) cells suggest a position downstream of Zap-70 in the pathway. Through Western blot analysis of TCR-stimulated P116 (Zap-70 null) cells, previous studies have shown decreases in tyrosine phosphorylation on proteins such as PLCγ1, LAT, and Erk1/2 (25, 27, 28). Our SILAC quantitation results also showed decrease in phosphorylation on these downstream proteins in Zap-70 null cells at PLCγ1 (Tyr-771, significantly decreased at 2 min, p value < 0.05), LAT (Tyr-45, significantly decreased at 2 min, p value < 0.05), Erk1 (Tyr-204, significantly decreased at 7 and 10 min, p value < 0.05), Erk2 (Tyr-187, significantly decreased at 0 and 2 min, p value < 0.05).

Although phosphorylation sites upstream of Zap-70 would be expected to be unaffected by Zap-70 removal, three tyrosine residues within the TCR CD3ζ (Tyr-111, Tyr-72, Tyr-142) immunoreceptor tyrosine activation motif (ITAM), along with three tyrosine residues on TCR CD3δ (Tyr-160, Tyr-149), and CD3ε (Tyr-199) ITAMs, decreased significantly (p value < 0.05 at various time points among these sites) in Zap-70 null cells (Fig. 5). These seemingly upstream perturbations in phosphorylation are, nevertheless, consistent with previous reports for the P116 Jurkat clone (39, 40). Although Lck-mediated phosphorylation of CD3ζ ITAMs is widely believed to precede Zap-70 recruitment and activation (41), previous studies have revealed a synergistic role of Zap-70-mediated recruitment as well as stabilization of the interaction between Lck and CD3ζ at the ITAM regions independent of Zap-70 kinase activity (Fig. 5*A*) (39, 40). Additional reports have indicated an essential role of Lck in the regulation of constitutive phosophorylation of CD3ζ (42). From these studies, it can be proposed that the removal of Zap-70 would result in a decrease of CD3ζ basal phosphorylation levels, which is consistent with our findings on these sites.

Novel Phosphorylation Sites Identified—The use of this quantitative approach to make comparisons between

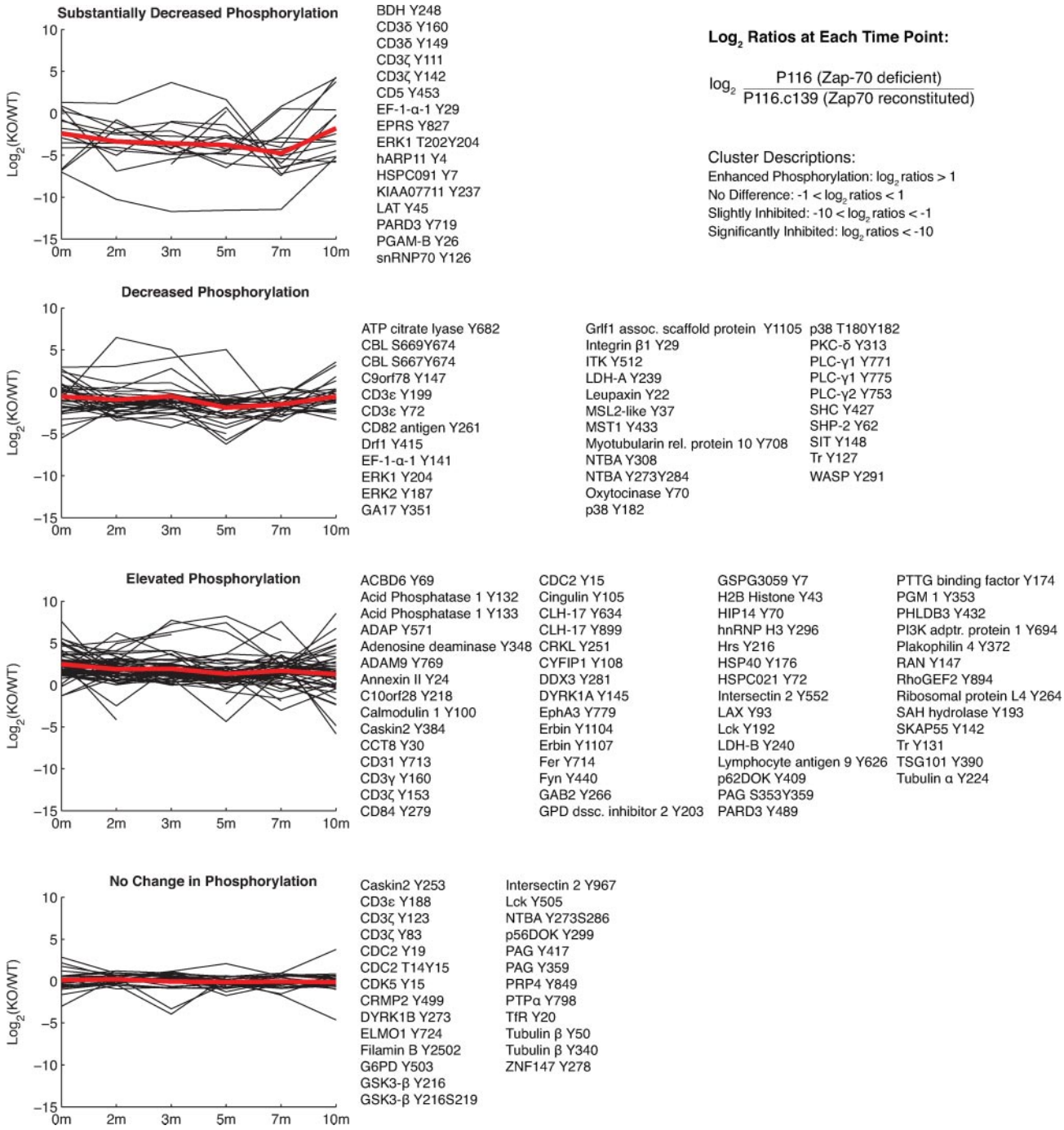

FIG. 4. **Classification of ZAP-70 null/reconstituted SILAC ratios.** The $\log_2$ SILAC ratios of Zap-70 null to Zap-70 reconstituted cells were classified into four major categories: Peptides with substantially decreased phosphorylation; peptides with decreased phosphorylation; peptides with elevated phosphorylation; peptides with no change in phosphorylation. SILAC ratios are calculated from the average of five replicate experiments.

Zap-70 null and reconstituted cells has also led to the generation of a broad test bed of novel, uncharacterized phosphorylation sites that can be positioned within the T cell signaling pathway. Among the 178 total unique phosphorylation sites identified in this analysis, 105 of these sites were found to be novel, *i.e.* sites that were previously uncharacterized in the Human Protein Reference Database Version 7. Furthermore, of the 105 newly discovered sites, 69 of these sites were changed significantly in abundance with Zap-70 removal. This data provides a wealth of information about the hypothetical placement of these sites relative to Zap-70 and the TCR (Fig. 6).

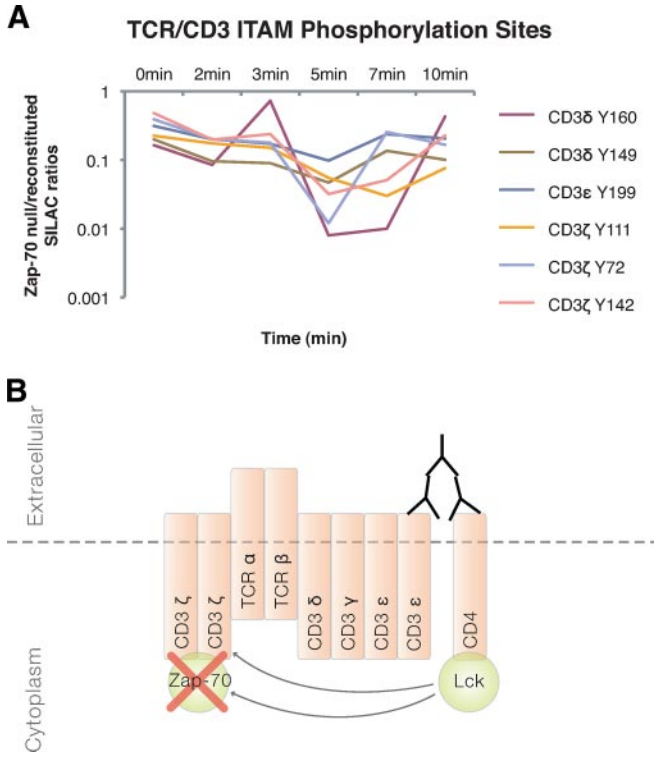

FIG. 5. **Lck phosphorylation of the CD3ζ ITAM motif requires Zap-70.** *A*, TCR/CD3 Zap-70 null/Zap-70 reconstituted SILAC ratio profiles. Differences in phosphopeptide abundance over time were represented as SILAC ratios between P116 (Zap-70 null) and P116.c139 (Zap-70 reconstituted) cells on CD3ζ, CD3ε, and CD3δ chains. SILAC ratios are calculated from the averages of five replicate experiments. *B*, model of Zap-70-dependent Lck phosphorylation of the CD3ζ ITAM motif as well as CD3/CD4 antibody co-stimulation.

DISCUSSION

The typical approach for elucidation of the structure of cellular signaling networks involves an iterative process of signaling protein disruptions and a large number of site-directed mutants, followed by characterization of every mutant through a battery of assays of cellular activation. One common phenotype employed to evaluate newly created signaling protein mutants is the use of phosphorylation site-specific Western blots. The advantage of this approach is the specificity of the measurement and the ease of quantitation of the change in phosphorylation. However, localization of protein phosphorylation events within signaling pathways requires two separate types of information: the precise timing of each phosphorylation site relative to receptor stimulation as well as the relationship of each phosphorylation site to canonical signaling pathway landmarks. Quantitative phosphoproteomics can provide a means to overcome some of these issues by providing a richer, unbiased site-specific view of the phosphoproteome of cells harboring altered signaling proteins. Quantitation methods, such as SILAC, can provide highly detailed information about differences between distinct populations, but the number of necessary quantitative comparisons quickly outpaces the number of available isotopically labeled amino acids. The combination of SILAC and label-free quantitation allows for a greatly increased number of receptor stimulation time points while providing highly accurate comparisons between signaling protein null and reconstituted cells at each time point using SILAC.

Mutant compensation could be a complicating factor in the interpretation of differences in phosphorylation between protein null and wild type cells. Downstream targets solely dependent on the removed protein for phosphorylation should show strong decreases in phosphorylation. However, if multiple pathways exist to phosphorylate a downstream target, a pathway independent of the removed protein may mask defects in the protein dependent pathway. For instance, in our analysis, the Zap-70 downstream target Thr-180, Tyr-182 of p38 MAPK showed only slight decreases in phosphorylation in Zap-70 null mutants stimulating the hypothesis of alternative pathways regulating this site and compensating for the loss of Zap-70. Phosphoproteomic data from isogenic mutant analysis must be interpreted with attention for the possibility of compensation.

The interpretation of phosphoproteomic data obtained by our method could also be complicated by the existence of positive and negative feedback regulatory loops within signaling pathways. Feedback mechanisms make placement of phosphorylation sites within the pathway difficult because they allow upstream components to also be altered by the removal of a protein. C-terminal Src kinase (Csk), CD45, casitas B-lineage lymphoma (c-cbl), and SHP-1 are proteins known to function in negative feedback mechanisms in TCR signaling (43–47). Positive feedback mechanisms have also been observed in T cells such as Erk phosphorylation of Lck (47–49). To face this challenge, a theoretical logical model was assembled to predict the effects of feedback inhibition or feedback activation upon SILAC ratios calculated with this method (Fig. 7). From this logical model, both feedback inhibition and activation would be expected to affect SILAC ratios of an upstream signaling protein phosphorylation site in a time-dependent manner, while direct downstream inhibition would be expected to decrease phosphorylation constitutively. Consistent with our feedback model, CD3ζ Tyr-123 followed the trends predicted for Zap-70-dependent feedback activation (significantly increased at 0 min (p value $<$ 0.05) followed by significantly decrease at 7 min (p value $<$ 0.05)), stimulating the hypothesis that this site may play a role in positive feedback that has not been previously characterized (Fig. 7*D*). This observation highlights the importance of studying the kinetics of the phosphoproteomes of isogenic mutants.

Additionally, for the majority of phosphorylation sites identified on the CD3γδζ subunits, we observed a gradual decrease in Zap-70 null/reconstituted SILAC ratios at early time points, followed by a gradual increase in Zap-70 null/recon-

Name	Site	0 min	2 min	3 min	5 min	7 min	10 min	Avg. SILAC Ratio
ACBD6	Y69	16.37				15.73		16.05
Actin	Y93	1.94	1.45			2.70		2.03
ADAM9	Y769	37.11						37.11
Adenosine deaminase	Y348			2.53			2.29	2.41
ATP1A1	Y260			1.76				1.76
ATP1A3	Y548	0.74						0.74
ATP1A3	Y549	0.74						0.74
BDH	Y248		0.06		0.14			0.10
C10orf28	Y218	1.48						1.48
CCT8	Y30		4.79					4.79
CD7	Y222				0.54			0.54
CD84	Y279	4.82	2.19		3.19			3.40
CLH-17	Y634	5.93		7.05		8.56		7.18
CLH-17	Y899	6.36	8.14	8.35	6.34	10.05	6.69	7.65
CRMP2	Y499		2.02			0.62		1.32
DDX3	Y281	3.49						3.49
DDX49	Y223					2.82		2.82
Drf1	Y415	0.20	0.33				0.45	0.33
DYRK1A	Y145		8.09					8.09
EF-1-α-1	Y141	1.70						1.70
Elongation Protein 3	Y329	1.86		2.49	1.97			2.11
Enolase 2	Y44					3.97		3.97
Erbin	Y1107		10.31	1.92				6.12
G6PD	Y503					0.30		0.30
GA17	Y351				0.18			0.18
GDP dissoc. inhibitor 2	Y203					3.54		3.54
Grlf1 assoc. scaffold protein	Y237	12.65						12.65
GSPG3059	Y188	57.33						57.33
H2B Histone	Y43	3.43	6.34				0.02	3.26
H4 Histone	Y52	1.26	1.36					1.31
hARP11	Y4				0.01			0.01
Hrs	Y216		3.92		3.36			3.64
HSP40	Y176		3.34					3.34
HSP90B	Y484	1.81						1.81
HSPC021	Y72						145.62	145.62

Name	Site	0 min	2 min	3 min	5 min	7 min	10 min	Avg. SILAC Ratio
Intersectin 2	Y552					2.63		2.63
LAT	Y45		0.26					0.26
LDH-A	Y239	11.41	10.11					10.76
LDH-B	Y240	6.62	9.93		3.52	6.63		6.68
MSL2-like 1	Y37		0.36		0.37			0.36
MST1	Y433					0.25		0.25
Myotubularin rel. protein 10	Y708	0.14				0.64		0.39
Nephrin like 1	Y724	2.27						2.27
NTBA	Y308					0.54		0.54
Oxytocinase	Y70				0.19			0.19
PARD3	Y489					3.18		3.18
PARD3	Y719		0.03					0.03
PGAM-B	Y26	2.49	2.28					2.39
PGM 1	Y353	6.26				7.31		6.79
PHLDB3	Y432	6.42	3.94	3.38	1.73			3.87
PI3K adaptor protein 1	Y694		69.91	100.84			38.37	69.71
PI4K α	Y1096	7.05	8.45			7.18		7.56
Plakophilin 4	Y372		9.58					9.58
PTTG binding factor	Y174		36.77	77.03		16.02		43.28
RA-GEF-2	Y1447		2.60	3.02				2.81
RAN	Y147		9.28	9.30	9.93	10.98		9.87
RCC1 like	Y215		0.19		0.05			0.12
RhoGEF2	Y894	11.73	13.16	23.77	6.29	6.40	2.89	10.71
SAH hydrolase	Y193	15.70	15.62					15.66
SKAP55	Y142			5.78			3.28	4.53
STS1	Y19	3.84	1.38	1.50				2.24
Syntenin 1	Y56		20.46					20.46
Tec tyrosine kinase	Y519		1.39					1.39
Thioredoxin reductase 1	Y131	2.74	3.32	4.95		5.66	2.98	3.93
Tubulin alpha 1	Y224	197.19				2.76	10.81	70.25
Tubulin beta 1	Y50	0.81					0.64	0.72
Tubulin beta 1	Y340						0.69	0.69
TSG 101	Y390	4.08		3.13		2.55		3.25
ZNF404	Y312	0.56				2.42		1.49

FIG. 6. **Dynamic effects of Zap-70 removal on novel phosphorylation sites discovered.** Listed in this table is a subset of phosphorylation sites identified, representing the novel sites that displayed significant changes in response to Zap-70. Novel sites are defined as sites that were previously uncharacterized in the Human Protein Reference Database Version 7. Also included are the SILAC ratios (Zap-70 null/reconstituted) for the time points that showed significant changes among the five replicate experiments (p value < 0.05) as well as the average SILAC ratio across all time points. If missing data because of the sensitivity limit of the instrument prevented the reproducible observation of SILAC ratios in at least three replicate experiments, or the null hypothesis cannot be rejected, then those squares are left *blank* in this table.

stituted SILAC ratios at later time points (Fig. 7*E2*). These trends are consistent with the hypothesis of competing positive and negative feedback loops functioning at different stages of stimulation. At early time points, positive feedback mechanisms could be regulating these sites, leading to a gradual decrease in Zap-70 null/reconstituted SILAC ratios. At later time points, negative feedback mechanisms could be regulating these same sites, leading to an increase in Zap-70 null/reconstituted SILAC ratios when Zap-70 is removed (Fig. 7*E1*). It has previously been shown that Erk positive and SHP-1 negative feedback pathways can compete to either activate or inhibit Lck function to allow for T cells to discriminate between self and foreign ligands (47).

To determine the biological significance of the 105 novel sites discovered in this study (Fig. 6), they must be placed within canonical pathways and networks of protein-protein interactions. Software tools that accelerate the assessment of existing protein knowledge and exploration of quantitative proteomic data in the context of protein interaction networks are essential. Although the primary literature may be investigated manually, the use of software enables enhanced efficiency. Current interactome database software is primarily web-based, and protein names must be searched one at a time. Because only proteins directly binding to the searched protein are revealed, the proteomics researcher must memorize the network to find longer range interactions. Existing website-driven protein-protein interaction queries do not allow searching by peptide sequence, leading to confusion arising from protein name ambiguity. Quantitative data must also be integrated in a manual fashion with the interactome network. Therefore, new proteomic data visual analysis tools are essential for tackling the overwhelming complexity of

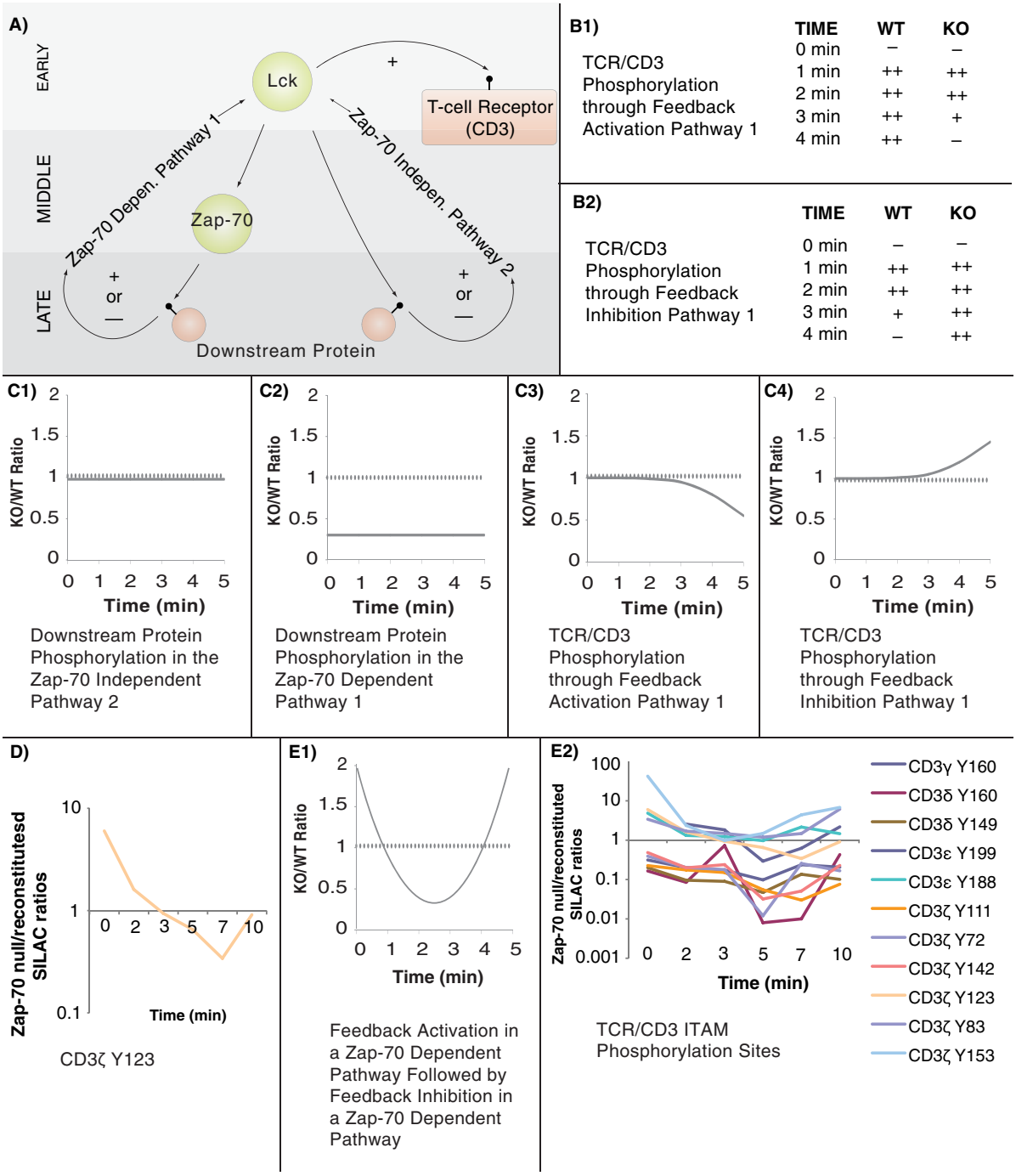

FIG. 7. **Theoretical model distinguishing direct inhibition from feedback regulation.** *A*, schematic model of pathway progression in response to T cell activation. At later stages, TCR signaling is regulated by either positive or negative feedback loop functions. Activation is represented by "+" while inhibition is represented by "−". Theoretical tables of expected wild type (*WT*) and knock-out (*KO*) TCR/CD3 phosphorylation temporal profiles for (*B1*) feedback activation and (*B2*) feedback inhibition (−, low level phosphorylation; +, moderate level phosphorylation; ++, high level phosphorylation. *B1*, with positive feedback through Zap-70, phosphorylation of CD3 would fail to be reduced at later time points in wild type cells compared with Zap-70 null cells. *B2*, with negative feedback through Zap-70, phosphorylation of CD3 would fail to be reduced at later time points in Zap-70 null cells compared with wild type cells. Expected changes in KO/WT SILAC ratios over time for (*C1*) TCR/CD3 in a Zap-70 independent pathway (SILAC ratio $\approx$ 1); (*C2*) downstream proteins affected by direct inhibition in a Zap-70-dependent pathway (SILAC ratio $<$ 1); (*C3*) positive feedback on CD3, and (*C4*) negative feedback on CD3. *Solid line* (–) corresponds to expected SILAC ratio profile. *D*, observed CD3ζ Tyr-123 Zap-70 null/Zap-70 reconstituted SILAC ratio profile. *E1*, predicted changes in KO/WT SILAC ratios over time for TCR/CD3 phosphorylation with feedback activation in a Zap-70-dependent pathway followed by feedback inhibition in a Zap-70 dependent pathway. *E2*, observed CD3ζγδε Zap-70 null/Zap-70 reconstituted SILAC ratios over time.

massive proteomic data sets and existing protein knowledge to gain insights into novel phosphorylation sites discovered in these types of studies.

We have recently developed phosphoproteomic exploration software with interactive visual integration of quantitative proteomic data, known signaling pathways, and protein-protein interaction networks to accelerate hypothesis generation, which is described in detail in an upcoming manuscript (www.peptidedepot.com/viz). Using this software, we examined the interactions between proteins observed to change in abundance in the Zap-70 null Jurkat cells. Although this analysis could have been accomplished through manual inspection of protein interactions described in hundreds of manuscripts, our newly developed software facilitates the assimilation of this information into a graphical representation of the T cell signaling pathway scaffold protein-protein interaction network. This depiction facilitates the rapid discovery of protein interactions among proteins observed in our data while providing rapid access to the underlying manuscripts through direct hyperlinks. A user may rapidly crawl through this interaction space in a dilated view that shows just a single protein and directly interacting proteins while maintaining global perspective of the T cell scaffold network (supplemental material 4). The quantitative phosphoproteomic data generated in this manuscript is provided as .pth input file for this software and is available for download without restriction (www.tcellpathway.com).

The ability to visualize our data in relation to the canonical T cell signaling pathway, focus on meaningful protein groups through the use of filters and selectors, and find possible pathways between multiple proteins with variable degrees of separation were integral in generating the hypotheses described in detail here. For example, this software has helped us to propose an unexpected hypothesis about the potential role of the pleckstrin homology domain (PH domain) of SKAP55 (Tyr-142). This site was observed to have slightly enhanced phosphorylation (significantly increased at 3 and 10 min, p value < 0.05) in Zap-70 null cells compared with its reconstituted counterpart in response to stimulation. Upon T cell activation, Fyn-associated SKAP55, in complex with the cytosolic adaptor protein ADAP, targets RAP1 GTPase to the plasma membrane to initiate cell adhesion (50–52). Although the mechanisms of SKAP55's interaction with Fyn and ADAP are well studied, the specific regulatory mechanisms of SKAP55's membrane targeting is still uncharacterized (50, 51). It has been established that the PH domain is involved in membrane recruitment for many cellular proteins (53). More recently, it has been shown that tyrosine phosphorylation of the PH domain of protein kinase D can serve in regulating protein function by possibly releasing the PH domain (undefined still whether it is from itself or the membrane), leading to its activation (54). Therefore, we hypothesize that phosphorylation at Tyr-142 of SKAP55 may lead to the inhibition of SKAP55's ability bind to the membrane, which would prevent RAP1 GTPase recruitment to the membrane and cell adhesion. The placement of a negatively charged phosphate group in the PH domain could impede the ability of SKAP55 to bind to polyphosphoinositides found at the membrane (53). Further investigation in the possible function of site Tyr-142 of SKAP55 is necessary to validate this hypothesis. The enhanced phosphorylation of Tyr-142 on SKAP55 that we observed could be explained by the misregulation of Fyn, a known regulator of SKAP55 (50, 52).

Our results also provide some insight on the possible function of NTBA in T cells. NTBA, an ITIM containing killer Ig-like receptor, has been previously shown to be expressed in all human NK, T, and B lymphocytes (55, 56). In NK cells, NTBA has been shown to display inhibitory functions by blocking the ability of NK cells to kill Epstein-Barr virus-infected target cells (55). Little is known about their role in T cells. Recently, certain KIRs (KIR2DL2 and KLRG1) have been shown to disrupt late T cell receptor-stimulated effector functions such the production of IFN-γ and interleukin-2, respectively (57, 58). Furthermore, site-directed mutagenesis of specific tyrosine residues in the ITIM motif of KLRG1 demonstrates the importance of tyrosine phosphorylation in the inhibitory process in T cells (58). In our results, the phosphorylation of site Tyr-308 located within the ITIM motif of NTBA was increased (significantly increased at 7min, p value < 0.05) in response to TCR cross-linking in Zap-70 reconstituted Jurkat cells, suggesting the involvement of NTBA in the T cell activation pathway. It is possible that NTBA, like other KIRs, functions to inhibit late T cell signaling events through phosphorylation of Tyr-308. Such a possibility warrants additional investigation to clearly define the role of site Tyr-308 of NTBA. We also observed a slightly decreased phosphorylation (significantly decreased at 7 min, p value < 0.05) of Tyr-308 in Zap-70 null cells suggesting that this site may be downstream of Zap-70 activation.

The quantitative phosphoproteomic isogenic mutant approach described here will not only provide greater insights into molecular mechanisms of the TCR signaling pathway, but also provide a generalized approach to elucidation of cell signaling pathways using phosphoproteomics. Although current phosphoproteomic studies have been impressive in their identification and quantitation of changes in phosphorylation abundance across large numbers of proteins (4, 9–12), the development of methodology capable of the multi-dimensional comparison of mutant and wild type cells through a time course of receptor stimulation is critically important. By combining genetic analysis and two well established proteomic quantitation methods, and novel visual analysis tools, our approach facilitates rapid elucidation of the biological significance of high throughput phosphoproteomic data. Comparison of data from removal of multiple signaling proteins at different positions within a single pathway (upstream, middle, and downstream) will provide a means of organizing hundreds to thousands of phosphoryl-

ation sites relative to canonical pathway signaling landmarks. Although our hybrid quantitation approach was applied to the analysis of wide-scale tyrosine phosphorylation here, it is generic in design and adaptable to a wide range of phosphopeptide enrichment strategies. Quantitative phosphoproteomic phenotyping of signaling protein mutants will be an ideal complement to traditional signaling approaches, accelerating understanding of the architecture of phosphorylation networks involved in a wide range of biological processes.

Acknowledgments—We thank K. Sauer at the Scripps Research Institute, Department of Immunology for his helpful discussions. We would also like to thank L. Samelson at the National Institute of Health for generously providing us with the Jurkat clones P116 (Zap-70 null) and P116.c139 (Zap-70 reconstituted).

* This work was supported, in whole or in part, by the National Institutes of Health Grant 2P20RR015578 and by a Beckman Young Investigator award.

S The on-line version of this article (available at http://www.mcponline.org) contains supplemental material.

§ These authors contributed equally to this work.

¶¶ To whom correspondence should be addressed: Ph.: 401-863-6091; Fax: 401-863-6087; E-mail: art@drsalomon.com; http://tcellpathway.com.

REFERENCES

1. Sickmann, A., Marcus, K., Schäfer, H., Butt-Dörje, E., Lehr, S., Herkner, A., Suer, S., Bahr, I., and Meyer, H. E. (2001) Identification of post-translationally modified proteins in proteome studies. *Electrophoresis* **22,** 1669–1676
2. Gygi, S. P., Corthals, G. L., Zhang, Y., Rochon, Y., and Aebersold, R. (2000) Evaluation of two-dimensional gel electrophoresis-based proteome analysis technology. *Proc. Natl. Acad. Sci. U. S. A.* **97,** 9390–9395
3. Beausoleil, S. A., Jedrychowski, M., Schwartz, D., Elias, J. E., Villén, J., Li, J., Cohn, M. A., Cantley, L. C., and Gygi, S. P. (2004) Large-scale characterization of HeLa cell nuclear phosphoproteins. *Proc. Natl. Acad. Sci. U. S. A.* **101,** 12130–12135
4. Ficarro, S. B., McCleland, M. L., Stukenberg, P. T., Burke, D. J., Ross, M. M., Shabanowitz, J., Hunt, D. F., and White, F. M. (2002) Phosphoproteome analysis by mass spectrometry and its application to *Saccharomyces cerevisiae*. *Nat. Biotechnol.* **20,** 301–305
5. Goshe, M. B., Conrads, T. P., Panisko, E. A., Angell, N. H., Veenstra, T. D., and Smith, R. D. (2001) Phosphoprotein isotope-coded affinity tag approach for isolating and quantitating phosphopeptides in proteome-wide analyses. *Anal. Chem.* **73,** 2578–2586
6. Olsen, J. V., Blagoev, B., Gnad, F., Macek, B., Kumar, C., Mortensen, P., and Mann, M. (2006) Global, *in vivo*, and site-specific phosphorylation dynamics in signaling networks. *Cell* **127,** 635–648
7. Posewitz, M. C., and Tempst, P. (1999) Immobilized gallium(III) affinity chromatography of phosphopeptides. *Anal. Chem.* **71,** 2883–2892
8. Luo, Q., Tang, K., Yang, F., Elias, A., Shen, Y., Moore, R. J., Zhao, R., Hixson, K. K., Rossie, S. S., and Smith, R. D. (2006) More sensitive and quantitative proteomic measurements using very low flow rate porous silica monolithic LC columns with electrospray ionization-mass spectrometry. *J. Proteome Res.* **5,** 1091–1097
9. Brill, L. M., Salomon, A. R., Ficarro, S. B., Mukherji, M., Stettler-Gill, M., and Peters, E. C. (2004) Robust phosphoproteomic profiling of tyrosine phosphorylation sites from human T cells using immobilized metal affinity chromatography and tandem mass spectrometry. *Anal. Chem.* **76,** 2763–2772
10. Cao, L., Yu, K., Banh, C., Nguyen, V., Ritz, A., Raphael, B. J., Kawakami, Y., Kawakami, T., and Salomon, A. R. (2007) Quantitative time-resolved phosphoproteomic analysis of mast cell signaling. *J. Immunol.* **179,** 5864–5876
11. Krüger, M., Kratchmarova, I., Blagoev, B., Tseng, Y. H., Kahn, C. R., and Mann, M. (2008) Dissection of the insulin signaling pathway via quantitative phosphoproteomics. *Proc. Natl. Acad. Sci. U. S. A.* **105,** 2451–2456
12. Schmelzle, K., Kane, S., Gridley, S., Lienhard, G. E., and White, F. M. (2006) Temporal dynamics of tyrosine phosphorylation in insulin signaling. *Diabetes* **55,** 2171–2179
13. Salomon, A. R., Ficarro, S. B., Brill, L. M., Brinker, A., Phung, Q. T., Ericson, C., Sauer, K., Brock, A., Horn, D. M., Schultz, P. G., and Peters, E. C. (2003) Profiling of tyrosine phosphorylation pathways in human cells using mass spectrometry. *Proc. Natl. Acad. Sci. U. S. A.* **100,** 443–448
14. Zhang, Y., Wolf-Yadlin, A., Ross, P. L., Pappin, D. J., Rush, J., Lauffenburger, D. A., and White, F. M. (2005) Time-resolved mass spectrometry of tyrosine phosphorylation sites in the epidermal growth factor receptor signaling network reveals dynamic modules. *Mol. Cell. Proteomics* **4,** 1240–1250
15. Ong, S. E., and Mann, M. (2005) Mass spectrometry-based proteomics turns quantitative. *Nat. Chem. Biol.* **1,** 252–262
16. Ong, S. E., Blagoev, B., Kratchmarova, I., Kristensen, D. B., Steen, H., Pandey, A., and Mann, M. (2002) Stable isotope labeling by amino acids in cell culture, SILAC, as a simple and accurate approach to expression proteomics. *Mol. Cell. Proteomics* **1,** 376–386
17. Ficarro, S. B., Salomon, A. R., Brill, L. M., Mason, D. E., Stettler-Gill, M., Brock, A., and Peters, E. C. (2005) Automated immobilized metal affinity chromatography/nano-liquid chromatography/electrospray ionization mass spectrometry platform for profiling protein phosphorylation sites. *Rapid Commun. Mass Spectrom.* **19,** 57–71
18. Germain, R. N., and Stefanová, I. (1999) The dynamics of T cell receptor signaling: complex orchestration and the key roles of tempo and cooperation. *Annu. Rev. Immunol.* **17,** 467–522
19. Samelson, L. E. (2002) Signal transduction mediated by the T cell antigen receptor: the role of adapter proteins. *Annu. Rev. Immunol.* **20,** 371–394
20. Weiss, A., Kadlecek, T., Iwashima, M., Chan, A., and Van Oers, N. (1995) Molecular and genetic insights into T-cell antigen receptor signaling. *Ann. N.Y. Acad. Sci.* **766,** 149–156
21. Abraham, R. T., and Weiss, A. (2004) Jurkat T cells and development of the T-cell receptor signaling paradigm. *Nat. Rev. Immunol.* **4,** 301–308
22. Finco, T. S., Kadlecek, T., Zhang, W., Samelson, L. E., and Weiss, A. (1998) LAT is required for TCR-mediated activation of PLCgamma1 and the Ras pathway. *Immunity* **9,** 617–626
23. Irvin, B. J., Williams, B. L., Nilson, A. E., Maynor, H. O., and Abraham, R. T. (2000) Pleiotropic contributions of phospholipase C-gamma1 (PLC-gamma1) to T-cell antigen receptor-mediated signaling: reconstitution studies of a PLC-gamma1-deficient Jurkat T-cell line. *Mol. Cell. Biol.* **20,** 9149–9161
24. Straus, D. B., and Weiss, A. (1992) Genetic evidence for the involvement of the lck tyrosine kinase in signal transduction through the T cell antigen receptor. *Cell* **70,** 585–593
25. Williams, B. L., Schreiber, K. L., Zhang, W., Wange, R. L., Samelson, L. E., Leibson, P. J., and Abraham, R. T. (1998) Genetic evidence for differential coupling of Syk family kinases to the T-cell receptor: reconstitution studies in a ZAP-70-deficient Jurkat T-cell line. *Mol. Cell. Biol.* **18,** 1388–1399
26. Yablonski, D., Kuhne, M. R., Kadlecek, T., and Weiss, A. (1998) Uncoupling of nonreceptor tyrosine kinases from PLC-gamma1 in an SLP-76-deficient T cell. *Science* **281,** 413–416
27. Shan, X., and Wange, R. L. (1999) Itk/Emt/Tsk activation in response to CD3 cross-linking in Jurkat T cells requires ZAP-70 and Lat and is independent of membrane recruitment. *J. Biol. Chem.* **274,** 29323–29330
28. Martelli, M. P., Lin, H., Zhang, W., Samelson, L. E., and Bierer, B. E. (2000) Signaling via LAT (linker for T-cell activation) and Syk/ZAP70 is required for ERK activation and NFAT transcriptional activation following CD2 stimulation. *Blood* **96,** 2181–2190
29. Griffith, C. E., Zhang, W., and Wange, R. L. (1998) ZAP-70-dependent and -independent activation of Erk in Jurkat T cells. Differences in signaling induced by H2o2 and Cd3 cross-linking. *J. Biol. Chem.* **273,** 10771–10776
30. Licklider, L. J., Thoreen, C. C., Peng, J., and Gygi, S. P. (2002) Automation of nanoscale microcapillary liquid chromatography-tandem mass spectrometry with a vented column. *Anal. Chem.* **74,** 3076–3083
31. Eng, J. A., McCormack, J. R., and Yates, J. R., 3rd (1994) An approach to correlate tandem mass spectral data of peptides with amino acid se-

quences in a protein database. *J. Am. Soc. Mass Spectrom.* **5,** 976–989
32. Yu, K., Sabelli, A., DeKeukelaere, L., Park, R., Sindi, S., Gatsonis, C. A., and Salomon, A. R. (2009) Integrated platform for high-throughput statistical and manual validation of tandem mass spectra. *Proteomics* **9,** 3115–3125
33. Elias, J. E., and Gygi, S. P. (2007) Target-decoy search strategy for increased confidence in large-scale protein identifications by mass spectrometry. *Nat. Methods* **4,** 207–214
34. Beausoleil, S. A., Villén, J., Gerber, S. A., Rush, J., and Gygi, S. P. (2006) A probability-based approach for high-throughput protein phosphorylation analysis and site localization. *Nat. Biotechnol.* **24,** 1285–1292
35. Robey, E., and Allison, J. P. (1995) T-cell activation: integration of signals from the antigen receptor and costimulatory molecules. *Immunol. Today* **16,** 306–310
36. Szamel, M., and Resch, K. (1995) T-cell antigen receptor-induced signal-transduction pathways–activation and function of protein kinases C in T lymphocytes. *Eur. J. Biochem.* **228,** 1–15
37. Ohteki, T., Parsons, M., Zakarian, A., Jones, R. G., Nguyen, L. T., Woodgett, J. R., and Ohashi, P. S. (2000) Negative regulation of T cell proliferation and interleukin 2 production by the serine threonine kinase GSK-3. *J. Exp. Med.* **192,** 99–104
38. Davidson, D., Bakinowski, M., Thomas, M. L., Horejsi, V., and Veillette, A. (2003) Phosphorylation-dependent regulation of T-cell activation by PAG/Cbp, a lipid raft-associated transmembrane adaptor. *Mol. Cell. Biol.* **23,** 2017–2028
39. Steinberg, M., Adjali, O., Swainson, L., Merida, P., Di Bartolo, V., Pelletier, L., Taylor, N., and Noraz, N. (2004) T-cell receptor-induced phosphorylation of the zeta chain is efficiently promoted by ZAP-70 but not Syk. *Blood* **104,** 760–767
40. Thome, M., Duplay, P., Guttinger, M., and Acuto, O. (1995) Syk and ZAP-70 mediate recruitment of p56lck/CD4 to the activated T cell receptor/CD3/zeta complex. *J. Exp. Med.* **181,** 1997–2006
41. Wange, R. L., and Samelson, L. E. (1996) Complex complexes: signaling at the TCR. *Immunity* **5,** 197–205
42. van Oers, N. S., Killeen, N., and Weiss, A. (1996) Lck regulates the tyrosine phosphorylation of the T cell receptor subunits and ZAP-70 in murine thymocytes. *J. Exp. Med.* **183,** 1053–1062
43. Bergman, M., Mustelin, T., Oetken, C., Partanen, J., Flint, N. A., Amrein, K. E., Autero, M., Burn, P., and Alitalo, K. (1992) The human p50csk tyrosine kinase phosphorylates p56lck at Tyr-505 and down regulates its catalytic activity. *EMBO J.* **11,** 2919–2924
44. Mustelin, T., Williams, S., Tailor, P., Couture, C., Zenner, G., Burn, P., Ashwell, J. D., and Altman, A. (1995) Regulation of the p70zap tyrosine protein kinase in T cells by the CD45 phosphotyrosine phosphatase. *Eur. J. Immunol.* **25,** 942–946
45. Murphy, M. A., Schnall, R. G., Venter, D. J., Barnett, L., Bertoncello, I., Thien, C. B., Langdon, W. Y., and Bowtell, D. D. (1998) Tissue hyperplasia and enhanced T-cell signaling via ZAP-70 in c-Cbl-deficient mice. *Mol. Cell. Biol.* **18,** 4872–4882
46. Plas, D. R., Johnson, R., Pingel, J. T., Matthews, R. J., Dalton, M., Roy, G., Chan, A. C., and Thomas, M. L. (1996) Direct regulation of ZAP-70 by SHP-1 in T cell antigen receptor signaling. *Science* **272,** 1173–1176
47. Stefanová, I., Hemmer, B., Vergelli, M., Martin, R., Biddison, W. E., and Germain, R. N. (2003) TCR ligand discrimination is enforced by competing ERK positive and SHP-1 negative feedback pathways. *Nat. Immunol.* **4,** 248–254
48. Altman, A., Kaminski, S., Busuttil, V., Droin, N., Hu, J., Tadevosyan, Y., Hipskind, R. A., and Villalba, M. (2004) Positive feedback regulation of PLCgamma1/Ca(2+) signaling by PKCtheta in restimulated T cells via a Tec kinase-dependent pathway. *Eur. J. Immunol.* **34,** 2001–2011
49. Mueller, D. L. (2003) Tuning the immune system: competing positive and negative feedback loops. *Nat. Immunol.* **4,** 210–211
50. Wu, L., Yu, Z., and Shen, S. H. (2002) SKAP55 recruits to lipid rafts and positively mediates the MAPK pathway upon T cell receptor activation. *J. Biol. Chem.* **277,** 40420–40427
51. Kliche, S., Breitling, D., Togni, M., Pusch, R., Heuer, K., Wang, X., Freund, C., Kasirer-Friede, A., Menasche, G., Koretzky, G. A., and Schraven, B. (2006) The ADAP/SKAP55 signaling module regulates T-cell receptor-mediated integrin activation through plasma membrane targeting of Rap1. *Mol. Cell. Biol.* **26,** 7130–7144
52. Wang, H., and Rudd, C. E. (2008) SKAP-55, SKAP-55-related and ADAP adaptors modulate integrin-mediated immune-cell adhesion. *Trends Cell Biol.* **18,** 486–493
53. Maffucci, T., and Falasca, M. (2001) Specificity in pleckstrin homology (PH) domain membrane targeting: a role for a phosphoinositide-protein co-operative mechanism. *FEBS Lett.* **506,** 173–179
54. Storz, P., Döppler, H., Johannes, F. J., and Toker, A. (2003) Tyrosine phosphorylation of protein kinase D in the pleckstrin homology domain leads to activation. *J. Biol. Chem.* **278,** 17969–17976
55. Bottino, C., Falco, M., Parolini, S., Marcenaro, E., Augugliaro, R., Sivori, S., Landi, E., Biassoni, R., Notarangelo, L. D., Moretta, L., and Moretta, A. (2001) NTB-A [correction of GNTB-A], a novel SH2D1A-associated surface molecule contributing to the inability of natural killer cells to kill Epstein-Barr virus-infected B cells in X-linked lymphoproliferative disease. *J. Exp. Med.* **194,** 235–246
56. Falco, M., Marcenaro, E., Romeo, E., Bellora, F., Marras, D., Vély, F., Ferracci, G., Moretta, L., Moretta, A., and Bottino, C. (2004) Homophilic interaction of NTBA, a member of the CD2 molecular family: induction of cytotoxicity and cytokine release in human NK cells. *Eur. J. Immunol.* **34,** 1663–1672
57. Henel, G., Singh, K., Cui, D., Pryshchep, S., Lee, W. W., Weyand, C. M., and Goronzy, J. J. (2006) Uncoupling of T-cell effector functions by inhibitory killer immunoglobulin-like receptors. *Blood* **107,** 4449–4457
58. Tessmer, M. S., Fugere, C., Stevenaert, F., Naidenko, O. V., Chong, H. J., Leclercq, G., and Brossay, L. (2007) KLRG1 binds cadherins and preferentially associates with SHIP-1. *Int. Immunol.* **19,** 391–400